Journal of Zhejiang University-SCIENCE B (Biomedicine & Biotechnology) *2022 23(10):863-875*
www.jzus.zju.edu.cn; www.springer.com/journal/11585
E-mail: jzus_b@zju.edu.cn

Research Article

https://doi.org/10.1631/jzus.B2200144

UPF1 increases amino acid levels and promotes cell proliferation in lung adenocarcinoma via the eIF2α-ATF4 axis

Lei FANG[1*], Huan QI[2*], Peng WANG[1], Shiqing WANG[1], Tianjiao LI[1], Tian XIA[2], Hailong PIAO[2✉], Chundong GU[1✉]

[1]*Department of Thoracic Surgery, Lung Cancer Diagnosis and Treatment Center of Dalian, The First Affiliated Hospital of Dalian Medical University, Dalian 116011, China*
[2]*CAS Key Laboratory of Separation Science for Analytical Chemistry, Dalian Institute of Chemical Physics, Chinese Academy of Sciences, Dalian 116023, China*

Abstract: Up-frameshift 1 (UPF1), as the most critical factor in nonsense-mediated messenger RNA (mRNA) decay (NMD), regulates tumor-associated molecular pathways in many cancers. However, the role of UPF1 in lung adenocarcinoma (LUAD) amino acid metabolism remains largely unknown. In this study, we found that UPF1 was significantly correlated with a portion of amino acid metabolic pathways in LUAD by integrating bioinformatics and metabolomics. We further confirmed that UPF1 knockdown inhibited activating transcription factor 4 (ATF4) and Ser51 phosphorylation of eukaryotic translation initiation factor 2α (eIF2α), the core proteins in amino acid metabolism reprogramming. In addition, UPF1 promotes cell proliferation by increasing the amino-acid levels of LUAD cells, which depends on the function of ATF4. Clinically, UPF1 mRNA expression is abnormal in LUAD tissues, and higher expression of UPF1 and ATF4 was significantly correlated with poor overall survival (OS) in LUAD patients. Our findings reveal that UPF1 is a potential regulator of tumor-associated amino acid metabolism and may be a therapeutic target for LUAD.

Key words: Up-frameshift 1 (UPF1); Activating transcription factor 4 (ATF4); Amino acid metabolism; Lung adenocarcinoma

1 Introduction

Lung cancer is the most deadly malignant tumor in the world, with 1.80 million deaths per year. With a high incidence rate of an estimated 2.21 million new cases each year, it accounts for 11.4% of all cancer cases (Sung et al., 2021; Zhou et al., 2021). Lung cancer includes two common types: non-small-cell lung cancer (NSCLC) and small-cell lung cancer (SCLC). Lung adenocarcinoma (LUAD) is the most common subtype of NSCLC, accounting for 85% of total diagnoses (Ferlay et al., 2015; Yu and Li, 2020).

Metabolic reprogramming is accompanied by tumor occurrence, development, and deterioration (Georgoudaki et al., 2016; Guo et al., 2021; Xia et al., 2021). Under the regulation of oncogenes, tumor cells actively absorb carbon and convert it into macromolecules that can be used as energy sources for intracellular adenosine triphosphate (ATP) production even in stressful environments (Li and Zhang, 2016; Dias et al., 2019; Sneeggen et al., 2020). In addition, the use of precursor molecules to promote synthesis of biomass provides a basis for the occurrence and development of tumors. It is worth noting that tumor-related metabolic reprogramming represents abnormal amino acid metabolism (Mossmann et al., 2018; Tabe et al., 2019), glucose metabolism (Abdel-Wahab et al., 2019; Peng et al., 2021), and lipid metabolism (Cao, 2019). Amino acids act as intermediates in the synthesis of proteins, lipids, and nucleic acids (Lieu et al., 2020). As a consequence, cancer cells have an increased requirement for amino acids to fuel their rapid proliferation. Amino acids can be divided into two classes (Li and Zhang, 2016): nonessential amino acids, such as glutamate, serine, glycine, and proline, and essential amino acids, such as arginine, leucine, and methionine.

✉ Chundong GU, guchundong@dmu.edu.cn
Hailong PIAO, hpiao@dicp.ac.cn
* The two authors contributed equally to this work
Chundong GU, https://orcid.org/0000-0002-2981-6578
Hailong PIAO, https://orcid.org/0000-0001-7451-0386

Received Mar. 18, 2022; Revision accepted June 2, 2022;
Crosschecked Sept. 1, 2022

In tumors, amino acids such as glutamine and aspartic acid can enter the tricarboxylic acid cycle for energy production (Lieu, et al., 2020). They are also important carbon sources for nucleotide synthesis in single-carbon metabolism (Newman and Maddocks, 2017). Additionally, amino acids balance redox reactions (Kawauchi et al., 2008) and participate in epigenetic regulation (Ulanovskaya et al., 2013; Lee et al., 2014). Therefore, both the synthesis and decomposition of amino acids affect the growth, proliferation, and invasion of tumor cells through a variety of pathways (Li and Yan, 2019; Zhu and Thompson, 2019). This makes it clear why it is necessary to explore the specific regulatory mechanism of amino acid metabolic reprogramming in lung adenocarcinoma.

Proteins regulating RNA play important roles in tumorigenesis and progression (Zhu et al., 2020). Nonsense-mediated messenger RNA (mRNA) decay (NMD) is a highly conserved mRNA monitoring process that removes abnormal transcripts containing premature terminators (Popp and Maquat, 2013; Lykke-Andersen and Jensen, 2015). It therefore acts as an mRNA quality control pathway to protect cells from the toxic effects of truncated protein produced by mRNA-containing premature terminators (Nicholson et al., 2010). In addition, NMD regulates a variety of biological development processes by controlling mRNA levels, including embryonic and brain development. NMD recognition of abnormal mRNA depends on the adenosine triphosphatase (ATPase) and hydrolase activities of up-frameshift 1 (UPF1) (Chen et al., 2021). Abnormal mRNA translation leads to aggregation of the polypeptide releasing factor eukaryotic release factor 1 (eRF1)/eRF3, which recruits UPF1 to bind UPF2 and UPF3 to form a complex that activates the NMD pathway (Dehecq et al., 2018). During NMD, UPF1 is phosphorylated by suppressor of morphogenesis in genitalia 1 (SMG1) and inhibited by SMG8/9, thereby mediating the degradation of NMD substrates through this phosphorylation/dephosphorylation cycle (Kurosaki et al., 2019). With the development of research, it has been found that UPF1 plays a crucial role in multiple types of tumors, including pancreatic cancer (Liu et al., 2014), gastric cancer (Li et al., 2017), hepatocellular cancer (Chang et al., 2016), ovarian cancer (Pei et al., 2019), and thyroid cancer (Zhong et al., 2020).

Activating transcription factor 4 (ATF4) belongs to a family of DNA-binding proteins that includes the activating protein-1 (AP-1) family of transcription factors and cyclic adenosine monophosphate (cAMP)-response element binding proteins (CREBs) (Hai and Curran, 1991). It is widely known as a key oncogene in metabolic reprogramming, especially in maintaining amino acid levels (Ameri and Harris, 2008). ATF4 target genes have been found to be critical for cell growth and cancer progression. Their activation depends on the phosphorylation of eukaryotic translation initiation factor 2α (eIF2α) at Ser51. The eIF2α-ATF4 axis plays a critical role in amino acid metabolic reprogramming of cancer cells, especially when cells are in a stressful nutrient-scarce microenvironment (B'chir et al., 2013; Bai et al., 2021).

The biological function of UPF1 in LUAD remains undefined, and there is no proof presented to explain the correlation between UPF1 and tumor metabolic reprogramming, so we synthetically analyzed proliferative capacity, metabonomics, and transcriptomics in LUAD cells when UPF1 expression was limited. The present study aimed to explore the functional role and regulatory mechanism of UPF1-participating metabolism in LUAD.

2 Materials and methods

2.1 Cell culture

The human LUAD cell lines H1299, A549, and HEK-293T cells were cultured in RPMI 1640 (GIBCO, USA) or Dulbecco's modified Eagle's medium (DMEM; GIBCO), each supplemented with 10% (volume fraction) fetal bovine serum (FBS; GIBCO) at 37 °C with 5% CO_2. The cell lines were obtained from the American Type Culture Collection (ATCC, Manassas, VA, USA).

2.2 Antibody and reagents

The following antibodies and reagents were used: anti-UPF1 (#12040, Cell Signaling Technology (CST), USA), anti-eIF2α (#5324, CST), anti-phospho-eIF2α (Ser51) (#3398, CST), anti-ATF4 (#ab184909, Abcam, USA), anti-vinculin (#SC-73614, Santa Cruz Biotechnology, USA), anti-rabbit (DA1E) monoclonal antibody (mAb) immunoglobulin G (IgG) (#3900, CST), protease inhibitors (#14001, Bimake, USA),

phosphatase inhibitors (#15001, Bimake), and MSTFA (#69479, Sigma, USA).

2.3 Plasmids

pCW57.1-Tet-UPF1WT was obtained from Addgene (#99146, USA). UPF1 and ATF4 complementary DNAs (cDNAs) (#HG11124-M, Sinobiological, China) were subcloned into pBoBi expression vectors which were cut by *Eco*RI and *Bam*HI. The expression vectors were produced by utilizing Exonuclease III (#M0206L, New England Biolabs, USA). Transfection was performed with Lipofectamine 2000 (Invitrogen, Carlsbad, CA, USA).

Lentiviral short hairpin RNA (shRNA) were cloned in pLKO.1 within the *Age*I/*Eco*RI sites at the 3' end of the human U6 promoter. The targeted sequences were as follows: shUPF1-1 (5'-GGCTTAGTCCATCAGCATC-3') and shUPF1-2 (5'-GCATCTTATTCTGGGTAATAA-3').

2.4 Construction of stable transfected cell lines

To package the virus, we seeded HEK-293T cells in a 6-cm dish at 60% density the previous day. Lipofectamine 2000 was used to co-transfect with the package plasmid psPAX2 and pVSVG. Cells needed nutritional support with 2 mL supplemental medium after 24 h. Then, 48 h after transfection, condition medium containing recombinant lentiviruses was collected and filtered with a 0.45-μm filter (Merck Millipore, Billerica, MA, USA). Supernatants from these samples were immediately administered to target cells along with Polybrene (Sigma-Aldrich, St. Louis, MO, USA) at a final concentration of 10 mg/mL, and the supernatants were incubated with the cells for 12 h. The stable cell lines were maintained with 2 μg/mL puromycin (InvivoGen, Pak Shek Kok, Hong Kong, China).

2.5 Western blot

Western blot analysis was performed with standard methods. Briefly, cells were lysed in RIPA buffer (#P0013B, Beyotime, China) containing protease inhibitors (B14001, Bimake) and phosphatase inhibitors (B15001, Bimake). Proteins were separated by sodium dodecyl sulfate-polyacrylamide gel electrophoresis (SDS-PAGE) and blotted onto a polyvinylidene fluoride (PVDF) membrane (Bio-Rad, Hercules, CA, USA). Membranes were probed with specific primary antibodies and then with peroxidase-conjugated secondary antibodies. Equal protein-sample loading was monitored using vinculin antibody. The bands were visualized by chemiluminescence (Fusion Fx, VILBER-LOUTMAT, France) or X-ray Film (#P14-A, BOTHCATKIN, China).

2.6 Colony formation assay

Cells were seeded into six-well plates with 500 cells per well and cultured 7 d for a two-dimensional colony-formation assay. Images were obtained using the Gel Image System (2500R, Tanon, Shanghai, China) and colony numbers were calculated by ImageJ (Version 1.8.0; https://imagej.nih.gov/ij).

2.7 Cell counting kit-8 assay

Cells were seeded into 96-well plates with 3000 cells and cultured for 5 d. Then, every other day, the solution from the cell counting kit-8 (CCK8, #HY-K0301, MedChemExpress, USA) was added to the cells to measure the number of viable cells. Briefly, the cells were incubated with 100 μL solution (10% (volume fraction) CCK8) per well for 2 h. The absorbance was measured at 450 nm using a multiplate reader. The results were calculated as mean±standard deviation (SD) of values from at least three individual experiments.

2.8 Flag-bead pulldown assay

HEK-293T cells were transfected with UPF1-Flag and lysed in NETN buffer for 60 min on ice. Lysates were centrifuged at 13 000*g* for 15 min at 4 °C. Liquid supernatant was incubated with anti-Flag affinity gel (#B23102, Bimake) for 6 h. The Flag-beads were washed five times with NETN buffer at 4 °C. Proteins were eluted by boiling in 1× SDS running buffer and subjected to SDS-PAGE for simple protein mixture identification.

2.9 Co-immunoprecipitation (Co-IP) assay

In brief, the cells were lysed by incubation with 700 μL lysis buffer and protease (#14001, Bimake) & phosphatase inhibitor (#15001, Bimake) cocktail at 4 °C for 1 h, followed by centrifugation at 13 000*g* for 15 min at 4 °C. The supernatant was harvested, of which 50 μL was reserved as the input group. The remaining samples were divided into two tubes: one was incubated with 2 μg anti-UPF1 and the other, acting as a negative control, was incubated with 2 μg of IgG. After incubation at 4 °C for 8 h, 20 μL of protein

A/G magnetic beads (#HY-K0202, MedChemExpress) was added to the mixture and incubated on a rotator overnight at 4 ℃. After washing five times, bead-bound proteins were eluted by denaturing in an appropriate amount of protein-loading buffer at 98 ℃ for 10 min and centrifuged; the supernatant was used for western blot analysis.

2.10 Total RNA isolation

In brief, TRIzol® LS (10296010, Thermofisher, USA) was used to lysate cells. We added 200 μL chloroform into 1.5 mL EP tube with collected cells and vortexed vigorously the solution. We then transferred 400 μL solution from the aqueous phase and added 400 μL isopropanol to initiate RNA precipitation. The RNA was pelleted by centrifuging and the pellets were washed with 800 μL ice-cold 75% (volume fraction) ethanol (in nuclease-free water). We centrifuged and removed the supernatant, and then air-dried the RNA pellets at room temperature. Lastly, we resuspended the pellets in nuclease-free water.

2.11 Gas chromatography-mass spectrometry analysis

The cells used for gas chromatography-mass spectrometry (GC-MS) analysis were promptly washed twice with cold PBS (HyClone, Utah, USA) and immediately quenched in liquid nitrogen, and then stored at −80 ℃ for GC-MS analysis before metabolite extraction.

GC-MS samples were prepared as previously described (Yan et al., 2019), with slight modifications. Briefly, 1 mL of methanol/water (4:1 (volume ratio), containing 10 μg/mL tridecanoic acid as an internal standard) solution was added to the cell-culture dish. Cells were quickly scraped into Eppendorf tubes (Eppendorf, Shanghai, China). Following vortexing and centrifugation, the supernatant of each sample and mixed quality control (QC) samples were lyophilized. After derivatization with methoxyamine pyridine followed by *N*-methyl-*N*-(trimethylsilyl)trifluoroacetamide (MSTFA), the prepared samples were centrifuged at 13 000*g* for 15 min at 4 ℃, and then the supernatants were used for GC-MS full-scan analysis.

2.12 Mouse subcutaneous tumorigenesis model

Pathogen-free male BALB/c athymic nude mice (4–6 weeks old) were randomly divided into groups. All mice were housed in specific-pathogen-free (SPF) environments. H1299 cells (5×10^6) were subcutaneously injected into the ipsilateral armpit of each mouse. Ten days after injection, tumor volumes (V=(width^2×length)/2) were measured using a caliper every 4 d. At Day 46, all mice were euthanized and the tumors were isolated.

2.13 KEGG and GSEA pathway enrichment analyses

Significantly different (P<0.05) metabolites in the GC-MS data of the UPF1 stable knockdown H1299 cells were subjected to Kyoto Encyclopedia of Genes and Genomes (KEGG) pathway enrichment analysis using MetaboAnalyst 5.0 (https://www.metaboanalyst.ca). Significantly different genes ($\log_2$FC>1, Q<0.05) in the transcriptome data of the cells were subjected to KEGG pathway enrichment analysis using the Database for Annotation, Visualization, and Integrated Discovery (DAVID) website (https://david.ncifcrf.gov). Gene Set Enrichment Analysis (GSEA) was performed by the cluster Profiler R package. Pathway information was obtained from the KEGG (https://www.kegg.jp).

2.14 Statistical analysis

We used the R studio and R packages (Version 3.3.3) to analyze LUAD tissue RNA-sequencing (RNA-seq) data from The Cancer Genome Atlas (TCGA) in HTSeq-FPKM format (https://portal.gdc.cancer.gov). The mean values of two groups were compared using Student's *t*-test, while the Kaplan-Meier test was used to calculate the differences in survival. After performing the Shapiro-Wilk normality test and Levene's test on the TCGA data, we used the independent sample *t*-test or Wilcoxon rank sum test. Bars and error represent the standard deviation (SD) of replicate measurements. The SPSS 18.0 software package (SPSS, Inc., Chicago, IL, USA) was used for statistical analysis.

3 Results

3.1 Effects of UPF1 on amino acid levels in lung adenocarcinoma

To explore the function of UPF1 in regulating metabolic reprogramming in lung adenocarcinoma, we constructed two stable UPF1 knockdown H1299 cell lines and performed GC-MS. We screened 36 differential metabolites in the shUPF1-1 group and 35 in

the shUPF1-2 group with the *P* value at less than 0.05. Twenty-eight metabolites were detected as appearing in both groups (Fig. 1a), and these were subjected to metabolic pathway analysis based on KEGG. Notably, the pathway "Valine, leucine, and isoleucine biosynthesis" showed the highest enrichment ratio (20), and eight of the top 25 pathways were directly related to amino acid metabolism (Fig. 1b). The metabolomics pathway enrichment analysis of these differentially expressed metabolites revealed a significant association between UPF1 and amino acid metabolism. To show the change in metabolites in detail, we

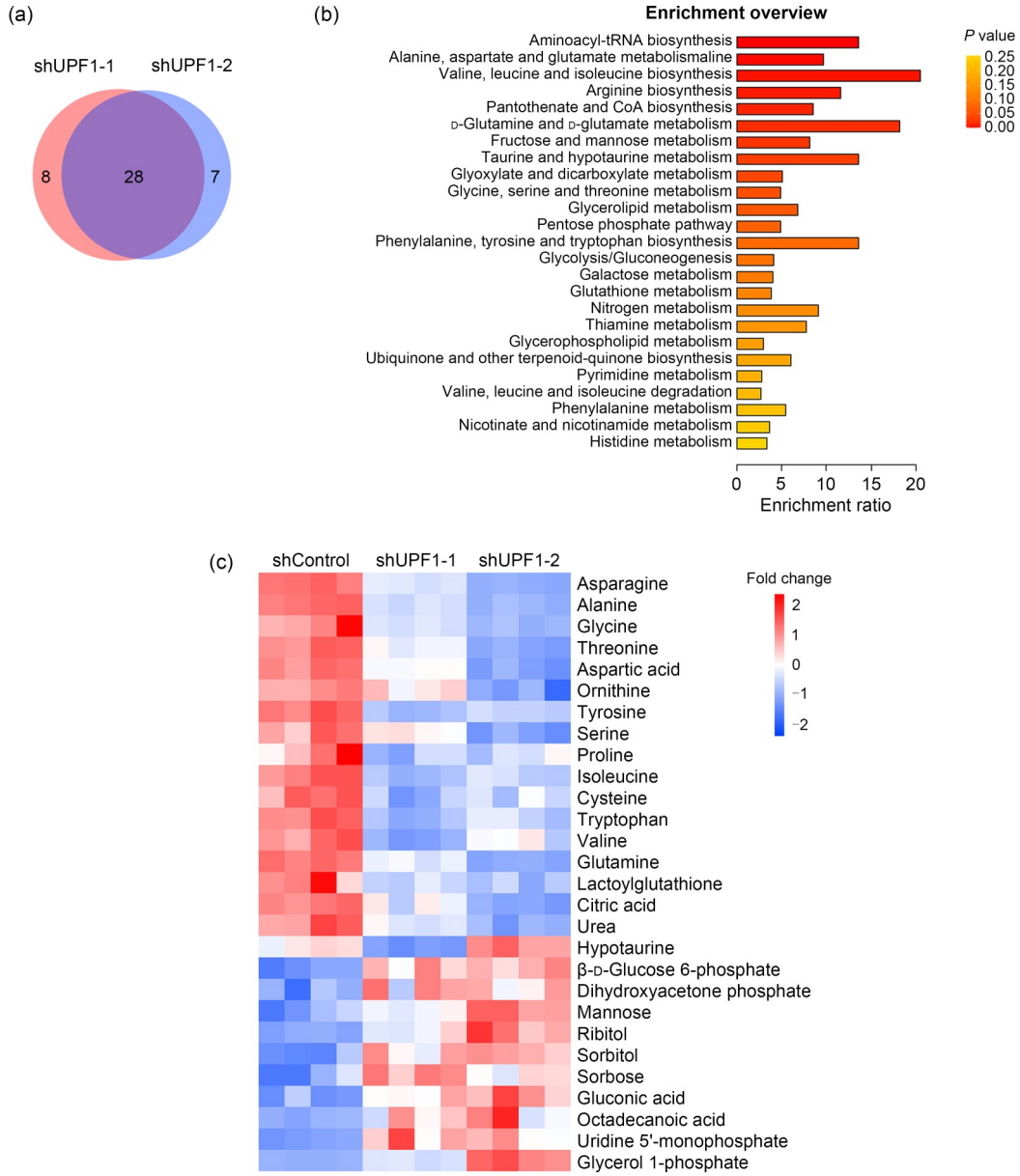

Fig. 1 Up-frameshift 1 (UPF1) knockdown in lung adenocarcinoma (LUAD) cells altered metabolomics profiling based on gas chromatography-mass spectrometry (GC-MS). (a) Venn diagram showing that 28 metabolites were detected in both UPF1-knockdown groups. (b) Kyoto Encyclopedia of Genes and Genomes (KEGG) pathway enrichment analysis differentially accumulated metabolites. The *y*-axis indicates the pathways, and the *x*-axis indicates the enrichment ratio in each pathway. The color bar indicates the corrected *P* value, with yellow representing a higher value and red representing a lower value. (c) Heatmap of the changes in metabolites related to UPF1 knockdown. Blue represents the decreasing trend, and red represents the increasing trend. From the regulatory trends in the heatmap, we observed that amino acids were the main downregulated components.

normalized the peak areas of each metabolite and listed the change in 28 metabolites as screened out in the form of a heatmap (Fig. 1c). Metabolites were classified and arranged according to the regulatory trends and signal category, in which the first 15 metabolites were related to amino acid metabolism and all showed downward trends. These results showed that the amino acid level of lung adenocarcinoma cells significantly decreased with UPF1 knockdown.

3.2 Regulation of ATF4 expression by UPF1 through eIF2α-Ser51 phosphorylation

To explore the specific mechanisms by which UPF1 promotes LUAD amino acid levels, we performed transcriptome sequencing in H1299 cells with stable UPF1 knockdown. We conducted KEGG pathway enrichment analysis for differentially expressed genes under $\log_2$FC>1 or $\log_2$FC<−1 and P<0.05 conditions. The analysis of these differentially expressed genes revealed a significant association between UPF1 and amino acid metabolism (Fig. 2a), including arginine and proline metabolism (fold enrichment=1.84, P=0.024, false discovery rate (FDR)=0.39) and glycine, serine, and threonine metabolism (fold enrichment=1.89, P=0.042, FDR=0.45). Our aim was to further decipher the molecular mechanisms involved in amino acid-related transcription regulated by UPF1. Subsequent GSEA confirmed that UPF1 knockdown significantly inhibits "Response of eIF2αK4 (GCN2) to amino acid deficiency" (NES=−3.429; Fig. 2b). Notably, the eIF2α-ATF4 axis is not only the most important part of the "eIF2αK4 (GCN2) to amino acid deficiency" pathway, but also a crucial factor regulating cell amino acid content. Activation of ATF4 expression depends upon eIF2α-Ser51 phosphorylation. We observed that silencing UPF1 drastically decreased ATF4 protein expression and phosphorylation at the Ser51 of eIF2α but had no effect on eIF2α expression (Fig. 2c).

To understand the specific mechanism by which the eIF2α-ATF4 axis is regulated, we transfected control and UPF1-Flag overexpression vectors into HEK-293T cells. The data from simple protein mixture identification suggested that UPF1 may interact with EIF2S1, also known as the subunit α of eIF2 (eIF2α) (Fig. 2d). Co-immunoprecipitation (Co-IP) assays showed that UPF1 was significantly bound to eIF2α in H1299 cells (Fig. 2e). In summary, these data indicated that UPF1 knockdown significantly inhibited phosphorylation of eIF2α-Ser51 and expression of ATF4 protein, thereby downregulating the intracellular amino acid level in lung adenocarcinoma cells.

3.3 Regulation of amino acid levels by UPF1 depending upon ATF4 expression in LUAD cells

Previous data have confirmed that the amino acid level is maintained by UPF1. Accordingly, we performed GC-MS experiments to further verify that ATF4 was involved in UPF1-induced amino acid metabolism reprogramming. Knockdown of UPF1 reduced the levels of diverse amino acids; conversely, ATF4 overexpression rescued the amino acid levels in UPF1-knockdown LUAD cells (Fig. 3a), including serine, threonine, aspartic acid, glutamine, tyrosine, glycine, isoleucine, alanine, and valine (Fig. 3b). These results indicate that ATF4 plays a critical role in UPF1-dependent amino acid metabolism reprogramming in LUAD.

3.4 Promotion of cell proliferation by UPF1 via ATF4 in vitro and in vivo

To evaluate the effect of ATF4 on cell proliferation by UPF1 inhibition, we rescued ATF4 expression in UPF1-knockdown cells (Fig. 4a). Colony formation and CCK-8 assays confirmed that ATF4 overexpression significantly increased the number of clones and proliferative potential in UPF1-knockdown H1299 and A549 cells (Figs. 4b–4d). In short, we confirmed that ATF4 recovered the suppressive effect of UPF1 deficiency on cell proliferation.

To simulate the growth environment of LUAD in vivo, we further carried out a subcutaneous tumorigenesis experiment in nude mice (Figs. 4e and 4f). In line with the observations in vitro, compared with the control group, the tumor mass and volume of the shUPF1-1 group were significantly reduced. Compared with the shUPF1-1 group, tumor mass and volume in the shUPF1-1+ATF4 overexpression group were significantly higher (Figs. 4g and 4h). In summary, these results suggest that oncogenic function of UPF1 may occur through ATF4 expression in LUAD.

3.5 Correlation of UPF1-ATF4 axis with poor prognosis in LUAD patients

To verify the high expression of UPF1 in LUAD tissues, we analyzed the mRNA expression level of

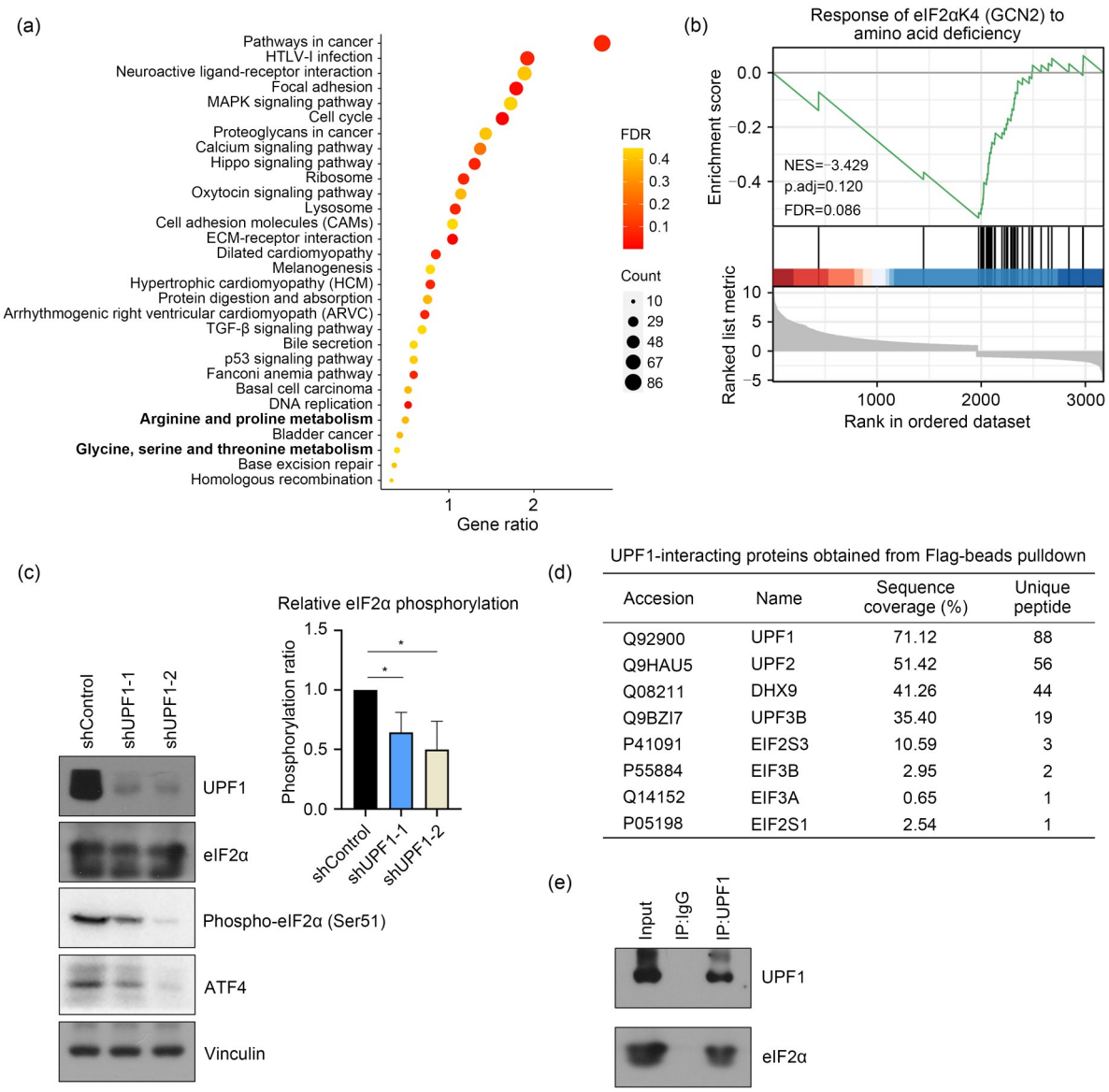

Accesion	Name	Sequence coverage (%)	Unique peptide
Q92900	UPF1	71.12	88
Q9HAU5	UPF2	51.42	56
Q08211	DHX9	41.26	44
Q9BZI7	UPF3B	35.40	19
P41091	EIF2S3	10.59	3
P55884	EIF3B	2.95	2
Q14152	EIF3A	0.65	1
P05198	EIF2S1	2.54	1

Fig. 2 Up-frameshift 1 (UPF1) knockdown inhibited Ser51 phosphorylation of eukaryotic translation initiation factor 2α (eIF2α) and activating transcription factor 4 (ATF4) expression. (a) Kyoto Encyclopedia of Genes and Genomes (KEGG) pathway enrichment analysis of differentially expressed genes based on transcriptome sequencing of UPF1 knockdown in H1299 cells. The *y*-axis indicates the pathway names, and the *x*-axis indicates the gene ratio in each pathway. Bubble size indicates the number of genes. The color bar indicates the corrected false discovery rate (FDR) value with yellow representing a higher value and red a lower value. (b) Gene set enrichment analysis (GSEA) was performed in the shUPF1-1 groups based on the transcriptome sequencing dataset. A positive enrichment score (ES) indicates gene set enrichment at the top of the ranked list; a negative ES (NES) indicates gene set enrichment at the bottom of the ranked list. The analysis demonstrates that known eIF2αK4 (GCN2) to amino acid deficiency was enriched. (c) Western blot analysis of the effects of UPF1 on eIF2α, eIF2α-Ser51, and ATF4 in H1299 cells, and quantitative analysis of eIF2α-Ser51/eIF2α ratio. Data are expressed as mean±standard deviation, n=3 ($^*P$<0.05). (d) Some of the proteins identified by simple protein mixture identification after the Flag-bead pulldown assay in UPF1-Flag overexpression (OE) 293T cells. (e) Western blot analysis of the co-immunoprecipitation (Co-IP) assay in H1299 wild-type cells. HTLV-I: human T-lymphotropic virus type I; ECM: extracellular matrix; TGF-β: transforming growth factor-β.

UPF1 in the TCGA database. UPF1 mRNA expression in tumors was significantly higher than in normal tissues (P=0.036; Fig. 5a). We subsequently constructed the Kaplan-Meier curve for LUAD patients using the TCGA database (n=535, best cutoff), which showed that a higher UPF1 level was associated with worse

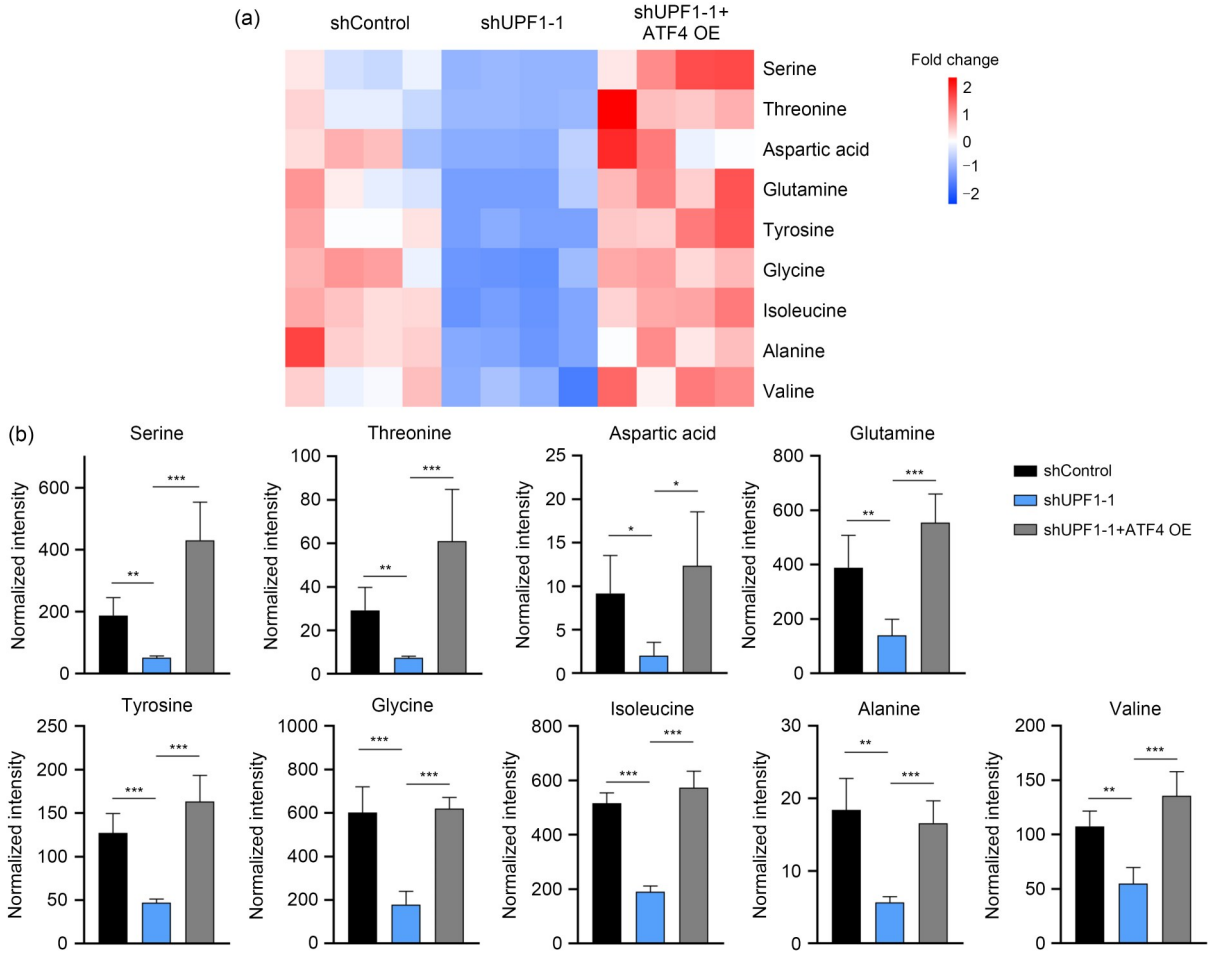

Fig. 3 Up-frameshift 1 (UPF1) knockdown inhibited lung adenocarcinoma (LUAD) cell proliferation via activating transcription factor 4 (ATF4) in vitro and in vivo. (a) Heatmap of the changes in amino acids related to ATF4 overexpression (OE) after UPF1 knockdown. Blue represents the decreasing trend and red represents a rising trend. (b) Bar diagram of changes in amino acids related to ATF4 OE after UPF1 knockdown. The bar height of the histogram indicates the mean of measurements of amino acids for each group in gas chromatography-mass spectrometry (GC-MS). Vertical bars are standard errors of the means. Data are expressed as mean±standard deviation, n=4. The star (*) symbol denotes the level of statistical significance determined by analysis of variance (ANOVA): * P<0.05, ** P<0.01, *** P<0.001.

overall survival (OS) (hazard ratio (HR)=1.38, P=0.038; Fig. 5b). However, the effect of ATF4 expression on OS was not statistically significant in LUAD patients (P=0.092; Fig. 5c). Then, we divided the cases into several groups according to the levels of UPF1 and ATF4 to explore whether ATF4 is involved in the function of UPF1 in worsening OS. As predicted, the OS of patients with high UPF1 and ATF4 expression was significantly lower than that of other patients (HR=0.70, P=0.023; Fig. 5d). In the group with high UPF1 expression, the OS of patients with high ATF4 expression was significantly lower than that of patients with low ATF4 expression (HR=0.63, P=0.024; Fig. 5e). However, in the cases with low UPF1 expression, there was no significant difference in OS between the low and high ATF4 expression groups (Fig. 5f). When the cases were classified by the expression level of ATF4 in the analysis, the UPF1 level no longer appeared to affect OS (Figs. 5g and 5h). These results indicated that UPF1 promoted tumor progression in an ATF4-dependent manner.

4 Discussion

More than a simple component that functions to regulate RNA degradation in cellular physiological processes, UPF1 is also relevant to multiple biological

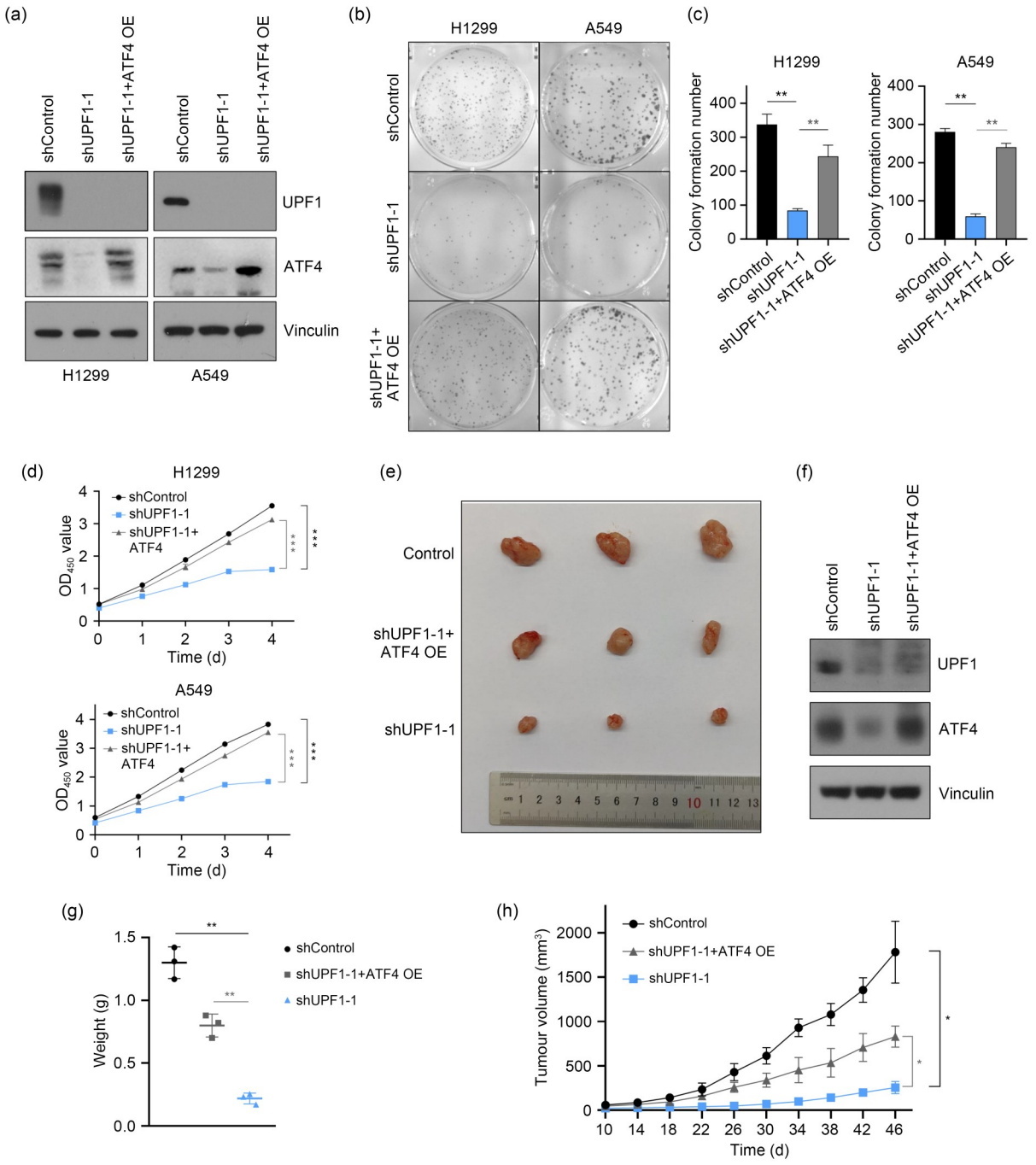

Fig. 4 Up-frameshift 1 (UPF1) enhanced amino acid levels depending upon activating transcription factor 4 (ATF4) in lung adenocarcinoma (LUAD) cells. (a) Western blot analysis of shUPF1-1 and shUPF1-1 with ATF4 overexpression (OE) in H1299 and A549 cells. (b, c) Clone formation assay results of the inhibitory effects of UPF1 deficiency and the rescue effects of ATF4 OE. (d) Cell counting kit-8 (CCK8) assay of cell viability. (e) Images of subcutaneous xenograft tumors (three per group). (f) Western blot analysis of protein expression levels of ATF4 and UPF1 in the subcutaneous xenograft tumors. (g) The weight of the subcutaneous xenograft tumors. (h) The volume changes of the subcutaneous xenograft tumors. Data are expressed as mean±standard deviation, n=3. The star (*) symbol denotes the level of statistical significance determined by analysis of variance (ANOVA): $^{*}P<0.05$, $^{**}P<0.01$, $^{***}P<0.001$. OD_{450}: optical density at 450 nm.

behaviors of tumors, such as proliferation (Han et al., 2020), apoptosis (Li et al., 2017), autophagy (Zhang et al., 2021), metastasis (Wang et al., 2019), and drug resistance (Zhang et al., 2017). Notably, UPF1

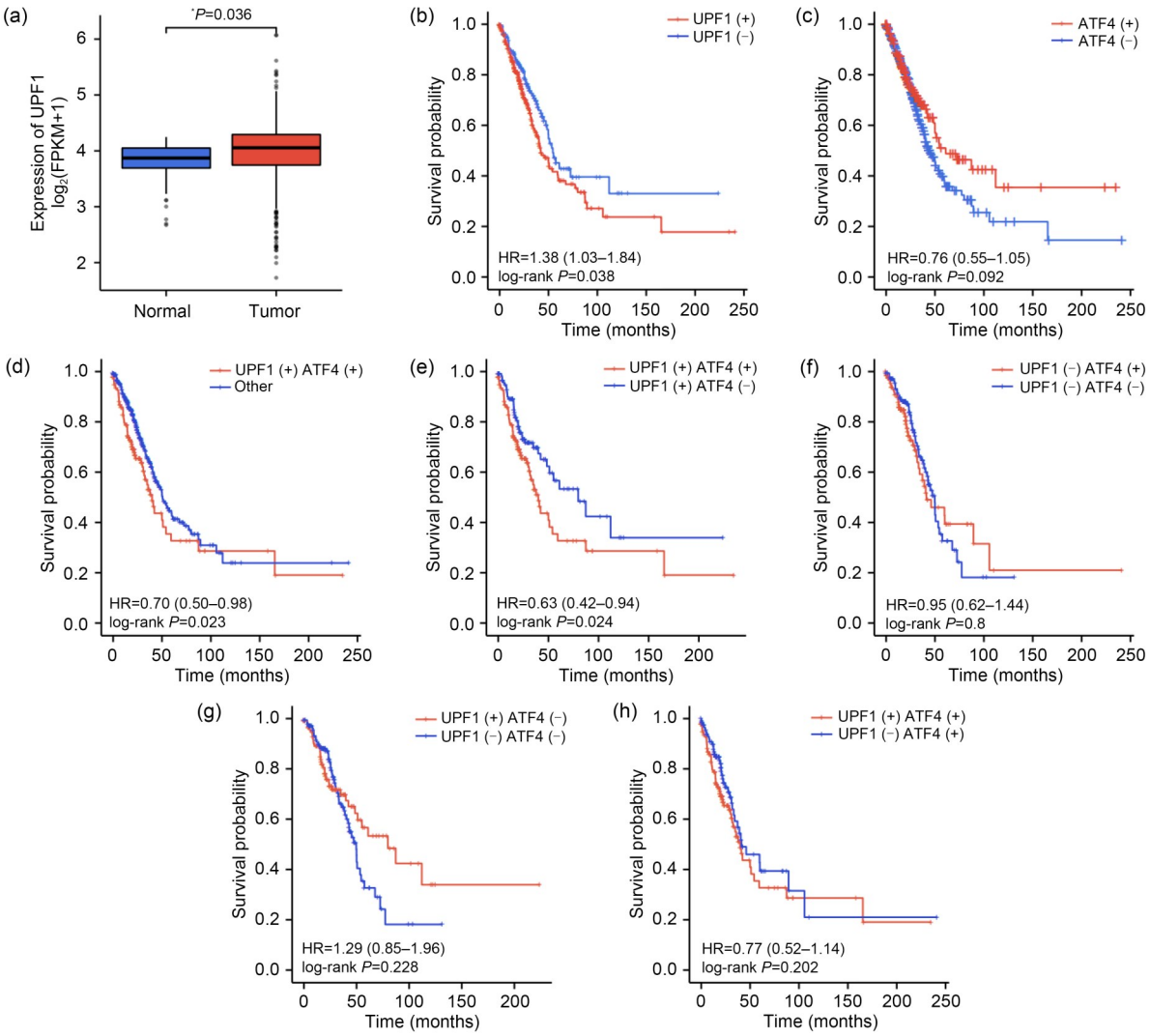

Fig. 5 Expression of up-frameshift 1 (UPF1) in lung adenocarcinoma (LUAD) tissues and its relationship with patient prognosis. (a) The messenger RNA (mRNA) expression of UPF1 in adjacent normal and LUAD tissues in The Cancer Genome Atlas (TCGA) database; (b, c) the relationship between UPF1 (b) or activating transcription factor 4 (ATF4) (c) expression and over survival (OS) in LUAD patients analyzed by Kaplan-Meier plotter. (d–h) To explore whether ATF4 is involved in the function of UPF1 in worsening OS, we divided the cases into several groups according to the levels of UPF1 and ATF4 and drew Kaplan-Meier curves. The "HR" and "log-rank *P*" of each group are listed under the curves ("+" represents high expression and "−" represents low expression after analysis with best cutoff). FPKM: fragments per kilobase per million; HR: hazard ratio.

exerts carcinogenic or anticarcinogenic effects depending on different pathological types. However, we found that proliferation of lung adenocarcinoma cells was suppressed upon UPF1 deficiency, but that the mechanism was undefined. In this study, we focused on the expression and prognosis of UPF1 in lung adenocarcinoma patients and explored the mechanism by which UPF1 promotes lung adenocarcinoma proliferation.

A growing appreciation of metabolic otherness in cancer has increased the demand to identify mechanisms that regulate metabolic reprogramming in tumors, mainly including glycol-metabolism, lipo-metabolism, and amino acid metabolism (Boroughs and Deberardinis, 2015; Chen et al., 2019; Zhu and Thompson, 2019). We hypothesized that UPF1 was associated with metabolic reprogramming in LUAD. In GC-MS-dependent metabolomics analysis, 28 metabolites were significantly disordered when UPF1 was knocked down, of which amino acids were the majority (Fig. 1). In addition to serving as substrates for protein synthesis, amino acids also play a role in energy generation, promoting nucleoside synthesis and maintaining redox

homeostasis in cells (Tsun and Possemato, 2015). A rich supply of amino acids is important for cancers to maintain their proliferation ability (Vettore et al., 2020). Our opinion, which remains to be confirmed, is that UPF1 promotes LUAD proliferation by means of amino acid metabolism reprogramming.

Tumor metabolic dysregulation is usually achieved by gene amplification or deletion or the altered activation status of upstream signaling pathways. However, no article has reported the relationship between UPF1 and tumor amino acid metabolism. Intracellular amino acid levels are regulated by several complex processes, including: synthesis of nonessential amino acids; import, export, and degradation of nonessential and essential amino acids; and protein synthesis and degradation. Previous studies have confirmed that ATF4 is a key transcription factor activating amino acid metabolism, for example the serine glycine metabolic pathway (Tajan et al., 2021) and asparagine synthetase (Gwinn et al., 2018), especially in nutrition deficiency or oxidative stress (Adams, 2007; Bai et al., 2021). The upstream open reading frame (uORF) in ATF4 mRNAs allows them to be translated by the 43S preinitiation complex in an eIF2α-dependent manner (Krishnamoorthy et al., 2019). In brief, eIF2α-ATF4 maintains intracellular amino acid levels via multiple mechanisms. Mechanistically, we found that UPF1 knockdown inhibited phosphorylation of eIF2α-Ser51 and further inhibited expression of ATF4, according to RNA-seq (Figs. 2a and 2b) and western blot results (Fig. 2c). These results suggest that UPF1 regulates amino acid levels via the eIF2α-ATF4 axis. The reprogramming of amino acid metabolism is a hallmark of cancer, which has an important impact on tumor proliferation (Hanahan and Weinberg, 2011). Both in vivo and in vitro experiments showed that UPF1 knockdown inhibited LUAD proliferation (Fig. 4), which was rescued by upregulation of amino acids activated by ATF4 overexpression (Fig. 3). In addition to survival analysis, patients with LUAD have a worse prognosis when UPF1 and ATF4 are both highly expressed (Fig. 5).

5 Conclusions

In summary, our study provided the key insight that UPF1, a critical factor of NMD, positively regulates ATF4 through activating eIF2α-Ser51 phosphorylation. Consequently, UPF1 promotes cell proliferation by increasing the amino acid levels of LUAD cells. These findings provide a new potential strategy for targeting UPF1 therapy in LUAD.

Acknowledgments

This work was supported by the National Natural Science Foundation of China (Nos. 81803886, 81774078, and 21907093). We thank members of the Dr. Hailong PIAO laboratory (Group 1821, Dalian Institute of Chemical Physics, Chinese Academy of Sciences, Dalian, China) for helpful discussion.

Author contributions

Lei FANG, Huan QI, and Peng WANG conceived the project, and designed and performed most of experiments and the data analysis. Hailong PIAO and Chundong GU supervised the project. Lei FANG and Shiqing WANG performed the establishment of animal models. Lei FANG, Huan QI, and Tianjiao LI provided significant intellectual input. Lei FANG, Huan QI, and Tian XIA wrote the manuscript with input from all other authors. All authors have read and approved the final manuscript, and therefore, have full access to all the data in the study and take responsibility for the integrity and security of the data.

Compliance with ethics guidelines

Lei FANG, Huan QI, Peng WANG, Shiqing WANG, Tianjiao LI, Tian XIA, Hailong PIAO, and Chundong GU declare that they have no conflict of interest.

All institutional and national guidelines for the care and use of laboratory animals were followed. All animal care and experimental procedures were approved by the Animal Care Ethics and Use Committee of Dalian Medical University (No. AEE19015).

References

Abdel-Wahab AF, Mahmoud W, Al-Harizy RM, 2019. Targeting glucose metabolism to suppress cancer progression: prospective of anti-glycolytic cancer therapy. *Pharmacol Res*, 150:104511. https://doi.org/10.1016/j.phrs.2019.104511

Adams CM, 2007. Role of the transcription factor ATF4 in the anabolic actions of insulin and the anti-anabolic actions of glucocorticoids. *J Biol Chem*, 282(23):16744-16753. https://doi.org/10.1074/jbc.M610510200

Ameri K, Harris AL, 2008. Activating transcription factor 4. *Int J Biochem Cell Biol*, 40(1):14-21. https://doi.org/10.1016/j.biocel.2007.01.020

Bai XP, Ni J, Beretov J, et al., 2021. Activation of the eIF2α/ATF4 axis drives triple-negative breast cancer radioresistance by promoting glutathione biosynthesis. *Redox Biol*, 43:101993. https://doi.org/10.1016/j.redox.2021.101993

B'chir W, Maurin AC, Carraro V, et al., 2013. The eIF2α/ATF4

pathway is essential for stress-induced autophagy gene expression. *Nucleic Acids Res*, 41(16):7683-7699. https://doi.org/10.1093/nar/gkt563

Boroughs LK, DeBerardinis RJ, 2015. Metabolic pathways promoting cancer cell survival and growth. *Nat Cell Biol*, 17(4):351-359. https://doi.org/10.1038/ncb3124

Cao YH, 2019. Adipocyte and lipid metabolism in cancer drug resistance. *J Clin Invest*, 129(8):3006-3017. https://doi.org/10.1172/JCI127201

Chang L, Li CC, Guo T, et al., 2016. The human RNA surveillance factor UPF1 regulates tumorigenesis by targeting Smad7 in hepatocellular carcinoma. *J Exp Clin Cancer Res*, 35:8. https://doi.org/10.1186/s13046-016-0286-2

Chen BL, Wang HM, Lin XS, et al., 2021. UPF1: a potential biomarker in human cancers. *Front Biosci (Landmark Ed)*, 26(5):76-84. https://doi.org/10.52586/4925

Chen PH, Cai L, Huffman K, et al., 2019. Metabolic diversity in human non-small cell lung cancer cells. *Mol Cell*, 76(5):838-851.e5. https://doi.org/10.1016/j.molcel.2019.08.028

Dehecq M, Decourty L, Namane A, et al., 2018. Nonsense-mediated mRNA decay involves two distinct Upf1-bound complexes. *EMBO J*, 37(21):e99278. https://doi.org/10.15252/embj.201899278

Dias AS, Almeida CR, Helguero LA, et al., 2019. Metabolic crosstalk in the breast cancer microenvironment. *Eur J Cancer*, 121:154-171. https://doi.org/10.1016/j.ejca.2019.09.002

Ferlay J, Soerjomataram I, Dikshit R, et al., 2015. Cancer incidence and mortality worldwide: sources, methods and major patterns in GLOBOCAN 2012. *Int J Cancer*, 136(5):E359-E386. https://doi.org/10.1002/ijc.29210

Georgoudaki AM, Prokopec KE, Boura VF, et al., 2016. Reprogramming tumor-associated macrophages by antibody targeting inhibits cancer progression and metastasis. *Cell Rep*, 15(9):2000-2011. https://doi.org/10.1016/j.celrep.2016.04.084

Guo X, Wang AM, Wang W, et al., 2021. HRD1 inhibits fatty acid oxidation and tumorigenesis by ubiquitinating CPT2 in triple-negative breast cancer. *Mol Oncol*, 15(2):642-656. https://doi.org/10.1002/1878-0261.12856

Gwinn DM, Lee AG, Briones-Martin-Del-Campo M, et al., 2018. Oncogenic KRAS regulates amino acid homeostasis and asparagine biosynthesis via ATF4 and alters sensitivity to L-asparaginase. *Cancer Cell*, 33(1):91-107.E6. https://doi.org/10.1016/j.ccell.2017.12.003

Hai T, Curran T, 1991. Cross-family dimerization of transcription factors Fos/Jun and ATF/CREB alters DNA binding specificity. *Proc Natl Acad Sci USA*, 88(9):3720-3724. https://doi.org/10.1073/pnas.88.9.3720

Han SH, Cao DD, Sha J, et al., 2020. LncRNA ZFPM2-AS1 promotes lung adenocarcinoma progression by interacting with UPF1 to destabilize ZFPM2. *Mol Oncol*, 14(5):1074-1088. https://doi.org/10.1002/1878-0261.12631

Hanahan D, Weinberg RA, 2011. Hallmarks of cancer: the next generation. *Cell*, 144(5):646-674. https://doi.org/10.1016/j.cell.2011.02.013

Kawauchi K, Araki K, Tobiume K, et al., 2008. p53 regulates glucose metabolism through an IKK-NF-κB pathway and inhibits cell transformation. *Nat Cell Biol*, 10(5):611-618. https://doi.org/10.1038/ncb1724

Krishnamoorthy GP, Davidson NR, Leach SD, et al., 2019. *EIF1AX* and *RAS* mutations cooperate to drive thyroid tumorigenesis through ATF4 and c-MYC. *Cancer Discov*, 9(2):264-281. https://doi.org/10.1158/2159-8290.CD-18-0606

Kurosaki T, Popp MW, Maquat LE, 2019. Quality and quantity control of gene expression by nonsense-mediated mRNA decay. *Nat Rev Mol Cell Biol*, 20(7):406-420. https://doi.org/10.1038/s41580-019-0126-2

Lee JV, Carrer A, Shah S, et al., 2014. Akt-dependent metabolic reprogramming regulates tumor cell histone acetylation. *Cell Metab*, 20(2):306-319. https://doi.org/10.1016/j.cmet.2014.06.004

Li XZ, Yan XH, 2019. Sensors for the mTORC1 pathway regulated by amino acids. *J Zhejiang Univ-Sci B (Biomed & Biotechnol)*, 20(9):699-712. https://doi.org/10.1631/jzus.B1900181

Li L, Geng Y, Feng R, et al., 2017. The human RNA surveillance factor UPF1 modulates gastric cancer progression by targeting long non-coding RNA MALAT1. *Cell Physiol Biochem*, 42(6):2194-2206. https://doi.org/10.1159/000479994

Li ZY, Zhang HF, 2016. Reprogramming of glucose, fatty acid and amino acid metabolism for cancer progression. *Cell Mol Life Sci*, 73(2):377-392. https://doi.org/10.1007/s00018-015-2070-4

Lieu EL, Nguyen T, Rhyne S, et al., 2020. Amino acids in cancer. *Exp Mol Med*, 52(1):15-30. https://doi.org/10.1038/s12276-020-0375-3

Liu C, Karam R, Zhou YQ, et al., 2014. The *UPF1* RNA surveillance gene is commonly mutated in pancreatic adenosquamous carcinoma. *Nat Med*, 20(6):596-598. https://doi.org/10.1038/nm.3548

Lykke-Andersen S, Jensen TH, 2015. Nonsense-mediated mRNA decay: an intricate machinery that shapes transcriptomes. *Nat Rev Mol Cell Biol*, 16(11):665-677. https://doi.org/10.1038/nrm4063

Mossmann D, Park S, Hall MN, 2018. mTOR signalling and cellular metabolism are mutual determinants in cancer. *Nat Rev Cancer*, 18(12):744-757. https://doi.org/10.1038/s41568-018-0074-8

Newman AC, Maddocks ODK, 2017. One-carbon metabolism in cancer. *Br J Cancer*, 116(12):1499-1504. https://doi.org/10.1038/bjc.2017.118

Nicholson P, Yepiskoposyan H, Metze S, et al., 2010. Nonsense-mediated mRNA decay in human cells: mechanistic insights, functions beyond quality control and the double-life of NMD factors. *Cell Mol Life Sci*, 67(5):677-700. https://doi.org/10.1007/s00018-009-0177-1

Pei CL, Fei KL, Yuan XY, et al., 2019. LncRNA DANCR

aggravates the progression of ovarian cancer by down-regulating UPF1. *Eur Rev Med Pharmacol Sci*, 23(24): 10657-10663. https://doi.org/10.26355/eurrev_201912_19763

Peng YY, Yang H, Li S, 2021. The role of glycometabolic plasticity in cancer. *Pathol Res Pract*, 226:153595. https://doi.org/10.1016/j.prp.2021.153595

Popp MWL, Maquat LE, 2013. Organizing principles of mammalian nonsense-mediated mRNA decay. *Annu Rev Genet*, 47:139-165. https://doi.org/10.1146/annurev-genet-111212-133424

Sneeggen M, Guadagno NA, Progida C, 2020. Intracellular transport in cancer metabolic reprogramming. *Front Cell Dev Biol*, 8:597608. https://doi.org/10.3389/fcell.2020.597608

Sung H, Ferlay J, Siegel RL, et al., 2021. Global cancer statistics 2020: GLOBOCAN estimates of incidence and mortality worldwide for 36 cancers in 185 countries. *CA Cancer J Clin*, 71(3):209-249. https://doi.org/10.3322/caac.21660

Tabe Y, Lorenzi PL, Konopleva M, 2019. Amino acid metabolism in hematologic malignancies and the era of targeted therapy. *Blood*, 134(13):1014-1023. https://doi.org/10.1182/blood.2019001034

Tajan M, Hennequart M, Cheung EC, et al., 2021. Serine synthesis pathway inhibition cooperates with dietary serine and glycine limitation for cancer therapy. *Nat Commun*, 12:366. https://doi.org/10.1038/s41467-020-20223-y

Tsun ZY, Possemato R, 2015. Amino acid management in cancer. *Semin Cell Dev Biol*, 43:22-32. https://doi.org/10.1016/j.semcdb.2015.08.002

Ulanovskaya OA, Zuhl AM, Cravatt BF, 2013. NNMT promotes epigenetic remodeling in cancer by creating a metabolic methylation sink. *Nat Chem Biol*, 9(5):300-306. https://doi.org/10.1038/nchembio.1204

Vettore L, Westbrook RL, Tennant DA, 2020. New aspects of amino acid metabolism in cancer. *Br J Cancer*, 122(2): 150-156. https://doi.org/10.1038/s41416-019-0620-5

Wang XK, Lai QH, He J, et al., 2019. Lncrna SNHG6 promotes proliferation, invasion and migration in colorectal cancer cells by activating TGF-β/Smad signaling pathway via targeting UPF1 and inducing EMT via regulation of ZEB1. *Int J Med Sci*, 16(1):51-59. https://doi.org/10.7150/ijms.27359

Xia LZ, Oyang LD, Lin JG, et al., 2021. The cancer metabolic reprogramming and immune response. *Mol Cancer*, 20:28. https://doi.org/10.1186/s12943-021-01316-8

Yan M, Qi H, Xia T, et al., 2019. Metabolomics profiling of metformin-mediated metabolic reprogramming bypassing AMPKα. *Metabolism*, 91:18-29. https://doi.org/10.1016/j.metabol.2018.11.010

Yu H, Li SB, 2020. Role of LINC00152 in non-small cell lung cancer. *J Zhejiang Univ-Sci B (Biomed & Biotechnol)*, 21(3):179-191. https://doi.org/10.1631/jzus.B1900312

Zhang H, You Y, Zhu ZL, 2017. The human RNA surveillance factor Up-frameshift 1 inhibits hepatic cancer progression by targeting MRP2/ABCC2. *Biomed Pharmacother*, 92: 365-372. https://doi.org/10.1016/j.biopha.2017.05.090

Zhang MF, Chen H, Qin P, et al., 2021. UPF1 impacts on mTOR signaling pathway and autophagy in endometrioid endometrial carcinoma. *Aging*, 13(17):21202-21215. https://doi.org/10.18632/aging.203421

Zhong ZB, Wu YJ, Luo JN, et al., 2020. Knockdown of long noncoding RNA DLX6-AS1 inhibits migration and invasion of thyroid cancer cells by upregulating UPF1. *Eur Rev Med Pharmacol Sci*, 24(16):8246. https://doi.org/10.26355/eurrev_202008_22587

Zhou L, Dong C, Xu Z, et al., 2021. NEDD8-conjugating enzyme E2 UBE2F confers radiation resistance by protecting lung cancer cells from apoptosis. *J Zhejiang Univ-Sci B (Biomed & Biotechnol)*, 22(11):959-965. https://doi.org/10.1631/jzus.B2100170

Zhu JJ, Thompson CB, 2019. Metabolic regulation of cell growth and proliferation. *Nat Rev Mol Cell Biol*, 20(7): 436-450. https://doi.org/10.1038/s41580-019-0123-5

Zhu W, Zhou BL, Rong LJ, et al., 2020. Roles of PTBP1 in alternative splicing, glycolysis, and oncogensis. *J Zhejiang Univ-Sci B (Biomed & Biotechnol)*, 21(2):122-136. https://doi.org/10.1631/jzus.B1900422